Inorganic Chemistry

Article

pubs.acs.org/IC

Crystal Structures and Raman Spectra of Imidazolium Poly[perfluorotitanate(IV)] Salts Containing the $[TiF_6]^{2-}$, $([Ti_2F_9]^-)_\infty$, and $[Ti_2F_{11}]^{3-}$ and the New $[Ti_4F_{20}]^{4-}$ and $[Ti_5F_{23}]^{3-}$ Anions

Igor M. Shlyapnikov,[†] Hélène P. A. Mercier,[‡] Evgeny A. Goreshnik,[†] Gary J. Schrobilgen,*[,‡] and Zoran Mazej*[,†]

[†]Department of Inorganic Chemistry and Technology, Jožef Stefan Institute, Jamova 39, SI-1000 Ljubljana, Slovenia

[‡]Department of Chemistry, McMaster University, Hamilton, Ontario L8S 4M1, Canada

Supporting Information

ABSTRACT: Reactions between imidazole (Im, $C_3H_4N_2$) and TiF_4 in anhydrous hydrogen fluoride (aHF) in different molar ratios have yielded $[ImH]_2[TiF_6]\cdot 2HF$, $[ImH]_3[Ti_2F_{11}]$, $[ImH]_4[Ti_4F_{20}]$, $[ImH]_3[Ti_5F_{23}]$, and $[ImH][Ti_2F_9]$ upon crystallization. All five structures were characterized by low-temperature single-crystal X-ray diffraction. The single-crystal Raman spectra of $[ImH]_4[Ti_4F_{20}]$, $[ImH]_3[Ti_5F_{23}]$, and $[ImH][Ti_2F_9]$ were also recorded and assigned. In the crystal structure of $[ImH]_2[TiF_6]\cdot 2HF$, two HF molecules are coordinated to each $[TiF_6]^{2-}$ anion by means of strong F−H···F hydrogen bonds. The $[Ti_2F_{11}]^{3-}$ anion of $[ImH]_3[Ti_2F_{11}]$ results from association of two TiF_6 octahedra through a common fluorine vertex. Three crystallographically independent $[Ti_2F_{11}]^{3-}$ anions, which have distinct geometries and orientations, are hydrogen-bonded to the $[ImH]^+$ cations. The $[ImH]_4[Ti_4F_{20}]$ salt crystallized in two crystal modifications at low (α-phase, 200 K) and ambient (β-phase, 298 K) temperatures. The tetrameric $[Ti_4F_{20}]^{4-}$ anion of $[ImH]_4[Ti_4F_{20}]$ consists of rings of four TiF_6 octahedra, which each share two *cis*-fluorine vertices, whereas the pentameric $[Ti_5F_{23}]^{3-}$ anion of $[ImH]_3[Ti_5F_{23}]$ results from association of five TiF_6 units, where four of the TiF_6 octahedra share two *cis*-vertices, forming a tetrameric ring as in $[Ti_4F_{20}]^{4-}$, and the fifth TiF_6 unit shares three fluorine vertices with three TiF_6 units of the tetrameric ring. The $[ImH][Ti_2F_9]$ salt also crystallizes in two crystal modifications at low (α-phase, 200 K) and high (β-phase, 298 K) temperatures and contains polymeric $([Ti_2F_9]^-)_\infty$ anions, which appear as two parallel infinite zigzag chains comprised of TiF_6 units, where each TiF_6 unit of one chain is connected to a TiF_6 unit of the second chain through a shared fluorine vertex. Quantum-chemical calculations at the B3LYP/SDDALL level of theory were used to arrive at the gas-phase geometries and vibrational frequencies of the $[Ti_4F_{20}]^{4-}$ and $[Ti_5F_{23}]^{3-}$ anions, which aided in the assignment of the experimental vibrational frequencies of the anion series.

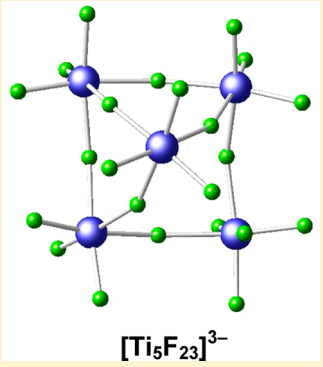

1. INTRODUCTION

Complex poly[perfluorotitanate(IV)] compounds are of interest because they are used as stereoselective catalysts in organic synthesis[1] and in reactions leading to olefin polymerization.[2] Two types of main-group titanium fluoride complexes exist: organometallic complexes with chemical bonds between titanium and organic molecules[3] and coordination complexes in which the fluorotitanate anions are coordinated to their cations through fluorine atoms.[4]

Among the many possible poly[perfluorotitanate(IV)] anions, $[Ti_xF_{4x+y}]^{y-}$ ($x, y \geq 1$), several have been synthesized, namely, $[TiF_6]^{2-}$,[5,6] $[Ti_2F_{10}]^{2-}$,[7,8] $[Ti_2F_{11}]^{3-}$,[9] $[Ti_4F_{18}]^{2-}$,[4,10] $([TiF_5]^-)_\infty$ (single chains),[11] $([Ti_2F_9]^-)_\infty$ (double chains),[4] $([Ti_3F_{13}]^-)_\infty$ (columns),[12] $([Ti_7F_{30}]^{2-})_\infty$ (columns),[13] and $([Ti_8F_{33}]^-)_\infty$ (layers).[14] Salts of the $[TiF_7]^{3-}$ anion are presently unknown. Salts that have been formulated as $Cs_3[TiF_7]$[15] and $[NH_4][Cu][TiF_7]\cdot 4H_2O$[16] are actually comprised of isolated $[TiF_6]^{2-}$ anions and a fluoride ion and are correctly formulated as $Cs_2[TiF_6]\cdot Cs[F]$[15,17] and $[Cu([H_2O]_4[TiF_6]]\cdot[NH_4][F]$.[18] The $[Ti_4F_{19}]^{3-}$ anion was recently isolated for the first time as the $[XeF_5]_3[Ti_4F_{19}]$ salt.[19]

In the present paper, crystallizations of imidazole (Im, $C_3H_4N_2$) and TiF_4 have been carried out in anhydrous hydrogen fluoride (aHF) and have yielded five imidazolium salts containing the $[TiF_6]^{2-}$, $[Ti_2F_{11}]^{3-}$, $[Ti_4F_{20}]^{4-}$, $[Ti_5F_{23}]^{3-}$, and $([Ti_2F_9]^-)_\infty$ anions. The salts have been isolated, and their crystal structures were determined and are described in the present paper. Although $[TiF_6]^{2-}$ salts are well-known, salts containing $([Ti_2F_9]^-)_\infty$ and $[Ti_2F_{11}]^{3-}$ are rare.[4,9] The $[Ti_4F_{20}]^{4-}$ anion represents a new example of a tetrameric anion comprised of four vertex-sharing octahedral TiF_6 units, whereas the $[Ti_5F_{23}]^{3-}$ anion is comprised of five vertex-sharing TiF_6 octahedra, providing a novel example of a pentameric poly[perfluorotitanate] anion. Quantum-chemical calculations have been used to compare the experimental geometries of $[Ti_4F_{20}]^{4-}$ and $[Ti_5F_{23}]^{3-}$ with their calculated gas-phase

Received: November 12, 2012
Published: July 9, 2013

   dx.doi.org/10.1021/ic302468j | *Inorg. Chem.* 2013, 52, 8315−8326

Table 1. Crystal Data and Refinement Results for Imidazolium Poly[perfluorotitanate(IV)] Salts Arising from Im−TiF_4−aHF Systems

	$[ImH]_2[TiF_6]\cdot 2HF$	$[ImH]_3[Ti_2F_{11}]$	β-$[ImH]_4[Ti_4F_{20}]^a$	α-$[ImH]_4[Ti_4F_{20}]^a$	$[ImH]_3[Ti_5F_{23}]$	β-$[ImH][Ti_2F_9]^a$	α-$[ImH][Ti_2F_9]^a$
fw (g/mol)	340.07	512.07	847.96	847.96	883.78	335.89	335.89
space group	$C2/c$	$C2/m$	$C2/m$	$P\bar{1}$	$Pna2_1$	$Pnma$	$P2_1/a$
a (Å)	14.437(8)	13.5371(2)	13.2139(4)	8.791(3)	22.0259(4)	5.3978(2)	5.3914(3)
b (Å)	7.436(4)	25.7451(4)	15.2096(7)	9.971(4)	10.2622(2)	12.2169(6)	15.4836(10)
c (Å)	13.261(8)	10.4139(2)	8.9514(3)	10.126(4)	12.3180(2)	15.2345(7)	11.9543(8)
α (deg)	90.00	90.00	90.00	118.808(8)	90.00	90.00	90.00
β (deg)	115.77(2)	100.980(1)	129.690(1)	92.366(3)	90.00	90.00	90.977(4)
γ (deg)	90.00	90.00	90.00	113.595(8)	90.00	90.00	90.00
V (Å^3)	1282.1(13)	3562.95(10)	1384.35(10)	681.8(5)	2784.29(9)	1004.63(8)	997.78(11)
Z	4	8	2	1	4	4	4
D_{calc} (g/cm^3)	1.762	1.909	2.034	2.065	2.108	2.221	2.236
T (K)	200	200	298	200	200	298	200
$R_1{}^b$	0.0882	0.0481	0.0518	0.0466	0.0317	0.0490	0.0655
$wR_2{}^c$	0.2181	0.1416	0.1561	0.1181	0.0898	0.1523	0.1576

[a]The symbols α and β correspond to the low- and high-temperature modifications, respectively, of $[ImH]_4[Ti_4F_{20}]$ and $[ImH][Ti_2F_9]$. [b]R_1 is defined as $\sum||F_o| - |F_c||/\sum|F_o|$ for $I > 2\sigma(I)$. [c]wR_2 is defined as $[\sum[w(F_o^2 - F_c^2)^2]/\sum w(F_o^2)^2]^{1/2}$ for $I > 2\sigma(I)$.

geometries. Their Raman spectra were assigned with the aid of the calculated frequencies and vibrational-mode descriptions.

2. RESULTS AND DISCUSSION

Crystal Structures of $[ImH]_2[TiF_6]\cdot 2HF$, $[ImH]_3[Ti_2F_{11}]$, $[ImH]_4[Ti_4F_{20}]$, $[ImH]_3[Ti_5F_{23}]$, and $[ImH][Ti_2F_9]$. The title salts were crystallized from aHF, providing single crystals from which their X-ray crystal structures were determined. The corresponding crystal data and refinement results are summarized in Table 1, geometrical parameters are summarized in Tables 2−4 and S1−S3 (Supporting Information), and packing diagrams are shown in Figures S1−S7 (Supporting Information) for $[ImH]_2[TiF_6]\cdot 2HF$, $[ImH]_3[Ti_2F_{11}]$, $[ImH]_4[Ti_4F_{20}]$, $[ImH]_3[Ti_5F_{23}]$, and $[ImH][Ti_2F_9]$.

(a) $[ImH]_2[TiF_6]\cdot 2HF$. The crystal structure of $[ImH]_2[TiF_6]\cdot 2HF$ consists of $[TiF_6]^{2-}$ anions and two HF solvent molecules that are coordinated to the F2 ligands of $[TiF_6]^{2-}$ by means of F−H···F hydrogen bonds, whereas the F3 and F1 ligands of $[TiF_6]^{2-}$ are more weakly hydrogen-bonded to $[ImH]^+$ cations (Figure 1). The $[ImH]^+$ cations are 2-fold-disordered. The Ti−F2 bonds are longer [1.908(4) Å] than the Ti−F3 [1.811(4) Å] and Ti−F1 [1.837(3) Å] bonds. The F4(H)···F2(−Ti) distance [2.374(6) Å] is shorter, i.e., the HF molecules are more strongly hydrogen-bonded than in $K_2CrF_6\cdot 2HF$ [F(−H)···F(−Cr), 2.455 Å].[20] Each $[TiF_6]^{2-}$ anion is coordinated to six $[ImH]^+$ cations, and the $[ImH]^+$ cations are each coordinated to three TiF_6 units through N−H···F and C−H···F hydrogen bonds.

(b) $[ImH]_3[Ti_2F_{11}]$. The crystal structure of $[ImH]_3[Ti_2F_{11}]$ consists of discrete $[Ti_2F_{11}]^{3-}$ anions in which two TiF_6 octahedra of $[Ti_2F_{11}]^{3-}$ share a common vertex (Figure 2). The Ti−F_t bond lengths range from 1.768(3) to 1.908(2) Å and from 1.9683(5) to 1.9805(6) Å for the Ti−F_b bond lengths (Table 2 and Figure 3) and are comparable to the corresponding bond lengths in $[C_5H_6N]_2[H_3O][Ti_2F_{11}]$ [Ti−F_t, 1.776(2)−1.880(2) Å; Ti−F_b, 1.9732(10) Å].[9]

In contrast with $[C_5H_6N]_2[H_3O][Ti_2F_{11}]$, where only one Ti_2F_{11} unit is defined,[9] there are three crystallographically independent Ti_2F_{11} units in $[ImH]_3[Ti_2F_{11}]$ which have different conformations and coordination spheres (Figures 2 and 3). The Ti_2F_{11} unit containing Ti1 is comprised of two symmetry-related octahedra with Ti1−F_b and Ti1−F_t bonds

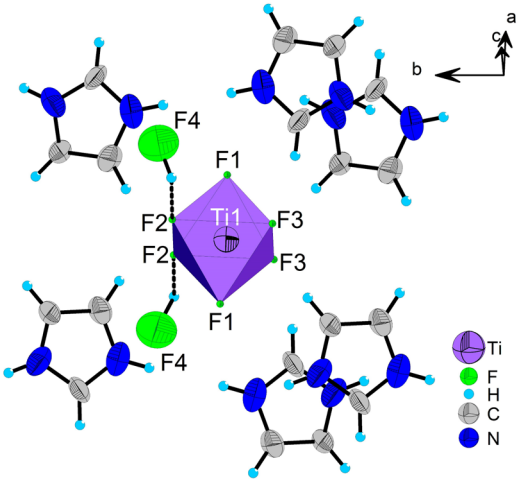

Figure 1. Crystal structure of $[ImH]_2[TiF_6]\cdot 2HF$ showing coordination of the hydrogen atoms of the HF molecules to the fluorine atoms of the $[TiF_6]^{2-}$ anion. Thermal ellipsoids are drawn at the 50% probability level. Only one of the two orientations of the disordered $[ImH]^+$ cations is depicted.

equal to 1.9805(6) and 1.796(4)−1.857(2) Å, respectively, and a Ti1−F_b−Ti1 angle of 180°. The equatorial TiF_4 planes of the TiF_6 octahedra of $[Ti_2F_{11}]^{3-}$ are eclipsed. The Ti_2F_{11} unit containing Ti2 is likewise comprised of two symmetry-related octahedra, but their TiF_4 planes have a gauche conformation with a dihedral angle of 8.50(6)° (Figure S8 in the Supporting Information). The Ti2−F_b bond [1.9683(5) Å] is longer than the Ti2−F_t bonds [1.792(2)−1.862(2) Å] and shorter than the corresponding Ti1−F_b bond, with a Ti2−F_b−Ti2 angle that is slightly bent [174.28(18)°]. The Ti_2F_{11} unit containing Ti3 has a Ti3−F_b bond length [1.9778(8) Å] that is very similar to the Ti1−F_b bond length [1.9805(6) Å] with a linear Ti3−F_b−Ti3 angle and eclipsed TiF_4 planes.

The coordination spheres formed by the $[ImH]^+$ cations of the three crystallographically independent $[Ti_2F_{11}]^{3-}$ anions differ with respect to their hydrogen-bonded contacts (Table S4 in the Supporting Information). The $[Ti1_2F_{11}]^{3-}$ anions are hydrogen-bonded to eight $[ImH]^+$ cations containing the non-disordered N3 and N4 atoms and the disordered N5/N5A and

dx.doi.org/10.1021/ic302468j | Inorg. Chem. 2013, 52, 8315−8326

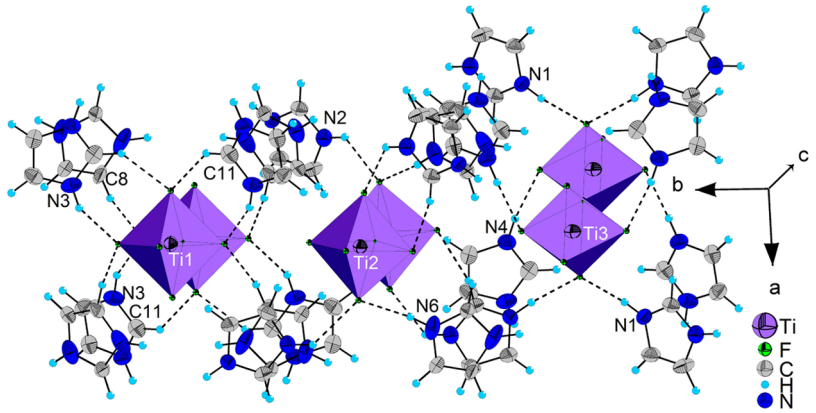

Figure 2. Crystal structure of $[ImH]_3[Ti_2F_{11}]$ showing coordination between the hydrogen atoms of the $[ImH]^+$ cations and the fluorine atoms of the $[Ti_2F_{11}]^{3-}$ anion. Thermal ellipsoids are drawn at the 50% probability level. Only one of the two orientations of the disordered $[ImH]^+$ cations is depicted.

Table 2. Experimental Geometrical Parameters of the Three Crystallographically Independent $[Ti_2F_{11}]^{3-}$ Anions in the Crystal Structure of $[ImH]_3[Ti_2F_{11}]$[a]

		Bond Lengths (Å)			
Ti1–F3	1.796(3)	Ti2–F9	1.792(2)	Ti3–F14	1.768(3)
Ti1–F2	1.849(3)	Ti2–F8	1.862(2)	Ti3–F13	1.908(2)
Ti1–F4	1.824(2)	Ti2–F11	1.841(2)	Ti3–F15	1.798(3)
Ti1–F5	1.857(2)	Ti2–F10	1.834(2)	Ti3–F16	1.847(2)
Ti1–F5A	1.857(2)	Ti2–F7	1.837(2)	Ti3–F16B	1.847(2)
Ti1–F1	1.9805(6)	Ti2–F6	1.9683(5)	Ti3–F12	1.9770(8)
		Bond Angles (deg)			
F3–Ti1–F2	93.55(15)	F9–Ti2–F8	93.73(9)	F14–Ti3–F13	89.55(13)
F3–Ti1–F4	93.63(14)	F9–Ti2–F11	93.36(9)	F14–Ti3–F15	96.56(16)
F3–Ti1–F5	93.00(6)	F9–Ti2–F10	94.11(10)	F14–Ti3–F16	94.90(7)
F3–Ti1–F5A	93.00(6)	F9–Ti2–F7	92.35(9)	F14–Ti3–F16B	94.90(7)
F3–Ti1–F1	179.38(11)	F9–Ti2–F6	179.01(11)	F14–Ti3–F12	176.17(12)
F2–Ti1–F4	172.82(12)	F8–Ti2–F11	172.92(8)	F13–Ti3–F15	173.89(14)
F2–Ti1–F5	89.52(5)	F8–Ti2–F10	88.62(7)	F13–Ti3–F16	86.92(6)
F2–Ti1–F5A	89.52(5)	F8–Ti2–F7	89.26(7)	F13–Ti3–F16B	86.92(6)
F2–Ti1–F1	85.83(10)	F8–Ti2–F6	86.78(6)	F13–Ti3–F12	86.61(8)
F4–Ti1–F5	90.10(5)	F11–Ti2–F10	90.95(7)	F15–Ti3–F16	92.54(5)
F4–Ti1–F5A	90.10(5)	F11–Ti2–F7	90.37(7)	F15–Ti3–F16B	92.54(5)
F4–Ti1–F1	86.99(9)	F11–Ti2–F6	86.13(6)	F15–Ti3–F12	87.28(12)
F5–Ti1–F5A	173.97(12)	F10–Ti2–F7	173.32(9)	F16–Ti3–F16B	168.37(14)
F5–Ti1–F1	87.00(6)	F10–Ti2–F6	86.75(11)	F16–Ti3–F12	84.90(7)
F5A–Ti1–F1	87.00(6)	F7–Ti2–F6	86.81(11)	F16B–Ti3–F12	84.90(7)
Ti1–F1–Ti1A	180.0	Ti2–F6–Ti2A	174.28(18)	Ti3–F12–Ti3A	180.0

[a]The atom-labeling schemes correspond to those used in Figure 3.

N6/N6A atoms [N3···F5, 2.813(3) Å; N5A···F2, 2.925(9) Å; C8···F5, 2.957(10) Å; C11···F4, 3.017(3) Å]. The $[Ti2_2F_{11}]^{3-}$ anions are hydrogen-bonded to six $[ImH]^+$ cations containing the N1 and N2 atoms and the disordered N5/N5A and N6/N6A atoms [N2···F11, 2.793(3) Å; N6···F8, 2.866(3) Å; C8A···F10, 2.868(4) Å]. Each $[Ti3_2F_{11}]^{3-}$ anion is hydrogen-bonded to eight non-disordered $[ImH]^+$ cations containing the N1 and N2 atoms and the N3 and N4 atoms [N4···F16, 2.743(3) Å; N1···F13, 2.749(2) Å; C1···F16, 2.996(4) Å]. The three Ti_2F_{11} units are pairwise coordinated so that $[Ti1_2F_{11}]^{3-}$ is bridged to $[Ti2_2F_{11}]^{3-}$ through $[ImH]^+$ cations containing N5/N5A and N6/N6A and to $[Ti3_2F_{11}]^{3-}$ through cations containing N3 and N4, whereas $[Ti2_2F_{11}]^{3-}$ is bridged to $[Ti3_2F_{11}]^{3-}$ through cations containing N1 and N2.

(c) $[ImH]_4[Ti_4F_{20}]$. The crystalline phase corresponding to an Im:TiF_4 molar ratio of 1:1 is formulated as $[ImH]_4[Ti_4F_{20}]$, where the $[Ti_4F_{20}]^{4-}$ anion has been structurally characterized for the first time. Examples of tetrameric metal fluoride species are rare. The first evidence for a tetramer comprised of four MF_6 octahedra sharing four vertices was provided by the ^{119}Sn and ^{19}F NMR spectra of "N_5SnF_5" in a HF solution, which yielded the gross geometry of the $[Sn_4F_{20}]^{4-}$ anion.[21] Two tetrameric perfluorotitanate salts, $[Ti_4F_{18}]^{2-}$ [4,10] and $[Ti_4F_{19}]^{3-}$,[19] and two tetrameric non-titanium compounds, $[C_6N_4H_{21}]_2[V_4O_4F_{14}]\cdot 3H_2O$[22] and $[CN_4H_8]_4[Zr_4F_{24}]\cdot 4H_2O$,[23] have been described in the literature. The $[V_4O_4F_{14}]^{6-}$ anion is comprised of four VOF_5 octahedra sharing two vertices and two edges, whereas the $[Zr_4F_{24}]^{8-}$ anion is comprised of four ZrF_8 square antiprisms sharing four edges.

The α- and β-phases of $[ImH]_4[Ti_4F_{20}]$ (the crystal structures were determined at 200 and 298 K, respectively) consist of tetrameric $[Ti_4F_{20}]^{4-}$ anions and $[ImH]^+$ cations that

dx.doi.org/10.1021/ic302468j | Inorg. Chem. 2013, 52, 8315–8326

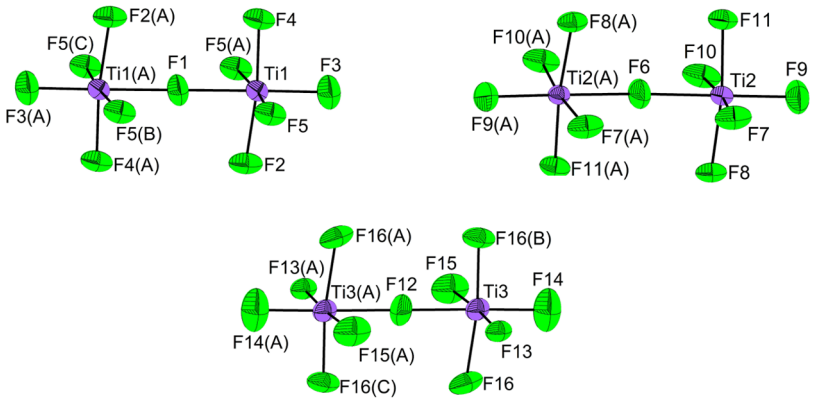

Figure 3. Experimental geometries of the $[Ti_2F_{11}]^{3-}$ anions in the crystal structure of $[ImH]_3[Ti_2F_{11}]$. Thermal ellipsoids are drawn at the 50% probability level.

interact through hydrogen bonds. The two $[ImH]^+$ cations defined in the β-phase are 2-fold disordered. The $[Ti_4F_{20}]^{4-}$ anion is comprised of four TiF_6 octahedra sharing two cis vertices (Figures 4 and 5). All titanium atoms in β-$[ImH]_4[Ti_4F_{20}]$ are situated in the same plane with four equal Ti···Ti distances [3.897(1) Å] and Ti···Ti···Ti angles close to 90° [Ti2···Ti1···Ti2, 94.2(2)°; Ti2···Ti1···Ti2, 85.8(2)°]. Each titanium atom is coordinated to two bridging and four terminal fluorine atoms. The Ti−F_t bond lengths range from 1.776(3) to 1.824(4) Å and are significantly shorter than the Ti−F_b bonds, i.e., Ti1−F_b, 1.956(2) Å; Ti2−F_b, 1.978(2) Å (Table 3).

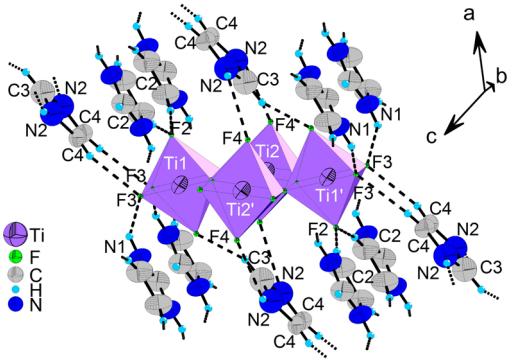

Figure 4. Crystal structure of β-$[ImH]_4[Ti_4F_{20}]$, determined at 298 K, showing coordination between the hydrogen atoms of the $[ImH]^+$ cations and the fluorine atoms of the $[Ti_4F_{20}]^{4-}$ anion. Thermal ellipsoids are drawn at the 50% probability level. Only one of the two orientations of the disordered $[ImH]^+$ cations is depicted.

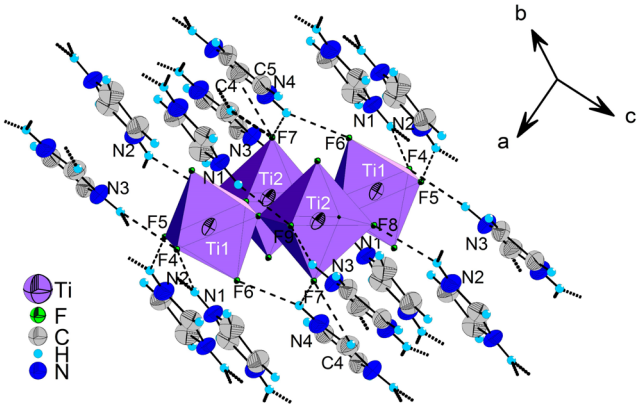

Figure 5. Crystal structure of α-$[ImH]_4[Ti_4F_{20}]$ determined at 200 K showing coordination between the hydrogen atoms of the $[ImH]^+$ cations and the fluorine atoms of the $[Ti_4F_{20}]^{4-}$ anion. Thermal ellipsoids are drawn at the 50% probability level.

Each $[Ti_4F_{20}]^{4-}$ anion is hydrogen-bonded to 12 $[ImH]^+$ cations, with N−H···F and C−H···F distances of 2.872(7)−3.093(22) and 2.836(13)−3.153(12) Å, respectively (Table S4 in the Supporting Information).

The Ti···Ti distances and Ti−F_t and Ti−F_b bond lengths in α-$[ImH]_4[Ti_4F_{20}]$ (Figure 5) are comparable to those in the β-modification [Ti···Ti, 3.854(1)−3.902(1) Å; Ti−F_t, 1.790(2)−1.840(2) Å; Ti−F_b, 1.965(2)−1.989(2) Å]. Each $[Ti_4F_{20}]^{4-}$ anion is hydrogen-bonded to 14 $[ImH]^+$ cations. Eight $[ImH]^+$ cations containing N1 and N2 atoms are hydrogen-bonded to different anions through one C−H···F [C1···F10, 2.990(4) Å] and four N−H···F [N2···F5, 2.847(4) Å; N2···F8, 2.936(4) Å; N1···F4, 2.839(3) Å; N1···F9, 2.977(4) Å] hydrogen bonds. The remaining six $[ImH]^+$ cations containing N3, N4, and C4 are coordinated to two $[Ti_4F_{20}]^{4-}$ anions through two N−H···F [N4···F6, 2.811(4) Å; N3···F9, 3.003(4) Å] hydrogen bonds and to two other anions through two N−H···F [N3···F4, 2.906(4) Å; N4···F7, 2.961(5) Å] and through one C−H···F [C4···F7, 2.935(5) Å] hydrogen bonds (Table S4 in the Supporting Information).

(d) $[ImH]_3[Ti_5F_{23}]$. The $[ImH]_3[Ti_5F_{23}]$ salt was obtained from a starting molar ratio of Im:TiF_4 = 1:1.67 (3:5). To the authors' knowledge, no pentameric units consisting of MX_n (X = F or F/O, n = 4−8) polyhedra have been reported thus far for organically templated metal fluorides.[24] The $[Ti_5F_{23}]^{3-}$ anion, which is comprised of five TiF_6 octahedra, represents a unique geometry among known pentameric polyanions comprised of octahedra. Each of four TiF_6 octahedra share two cis vertices with adjacent TiF_6 units, forming a tetrameric ring (Figure 6 and Table 4). The fifth TiF_6 unit shares three vertices with three octahedra of the tetrameric ring. All titanium atoms are crystallographically independent. Four of them (Ti2, Ti3, Ti4, and Ti5) are coordinated to three bridging and three terminal fluorine atoms. The unique Ti1 atom is coordinated to two cis-bridged and to four terminal fluorine atoms. The Ti−F_t and Ti−F_b bond length ranges are 1.757(3)−1.848(3) and 1.942(2)−2.014(2) Å, respectively. The $[Ti_5F_{23}]^{3-}$ anion is coordinated to six $[ImH]^+$ cations (three are crystallographically unique) through eight N−H···F [N···F, 2.805(4)−2.999(4) Å] and two C−H···F [C···F, 2.989(4)−2.995(4) Å]

dx.doi.org/10.1021/ic302468j | Inorg. Chem. 2013, 52, 8315−8326

Table 3. Experimental and Calculated Geometrical Parameters for the $[Ti_4F_{20}]^{4-}$ Anion

exptl[a,b]				calcd (D_{2d})[b,c]	
β-$[Ti_4F_{20}]^{4-}$		α-$[Ti_4F_{20}]^{4-}$			
Bond Lengths (Å)					
Ti1−F1	1.956(2)	Ti1−F1	1.965(2)	Ti1−F1	2.007
Ti1−F1A	1.956(2)	Ti1−F2	1.970(2)	Ti1−F2	2.007
Ti1−F2	1.807(4)	Ti1−F3	1.807(2)	Ti1−F3	1.839
Ti1−F3	1.793(3)	Ti1−F4	1.817(2)	Ti1−F4	1.842
Ti1−F3A	1.793(3)	Ti1−F5	1.793(2)	Ti1−F5	1.842
Ti1−F7	1.824(4)	Ti1−F6	1.840(2)	Ti1−F6	1.839
Ti2−F1	1.978(2)	Ti2−F1	1.989(2)	Ti2−F1	2.007
Ti2−F1B	1.978(2)	Ti2−F7	1.826(2)	Ti2−F7	1.839
Ti2−F4	1.803(3)	Ti2−F8	1.790(2)	Ti2−F8	1.842
Ti2−F4B	1.803(3)	Ti2−F9	1.800(2)	Ti2−F9	1.842
Ti2−F6	1.776(3)	Ti2−F10	1.800(2)	Ti2−F10	1.839
Ti2−F6B	1.776(3)	Ti2−F2A	1.989(2)	Ti2−F11	2.007
Bond Angles (deg)					
F1−Ti1−F1A	89.18(18)	F1−Ti1−F2	89.46(9)	F1−Ti1−F2	86.9
F1−Ti1−F2	86.35(14)	F1−Ti1−F3	86.47(10)	F1−Ti1−F3	88.9
F1−Ti1−F3A	178.06(15)	F1−Ti1−F4	177.75(10)	F1−Ti1−F4	177.5
F1−Ti1−F3	89.20(13)	F1−Ti1−F5	89.71(10)	F1−Ti1−F5	90.6
F1−Ti1−F7	86.92(13)	F1−Ti1−F6	87.09(9)	F1−Ti1−F6	88.9
F1A−Ti1−F2	86.35(14)	F2−Ti1−F3	86.22(9)	F2−Ti1−F3	88.9
F1A−Ti1−F3A	89.20(13)	F2−Ti1−F4	88.43(10)	F2−Ti1−F4	90.6
F1A−Ti1−F3	178.06(15)	F2−Ti1−F5	179.14(9)	F2−Ti1−F5	177.5
F1A−Ti1−F7	86.92(13)	F2−Ti1−F6	86.07(9)	F2−Ti1−F6	88.9
F2−Ti1−F3A	92.49(13)	F3−Ti1−F4	92.37(10)	F3−Ti1−F4	91.1
F2−Ti1−F3	92.49(13)	F3−Ti1−F5	93.95(10)	F3−Ti1−F5	91.1
F2−Ti1−F7	170.54(19)	F3−Ti1−F6	170.14(10)	F3−Ti1−F6	176.9
F3A−Ti1−F3	92.41(20)	F4−Ti1−F5	92.40(10)	F4−Ti1−F5	91.9
F3A−Ti1−F7	94.05(13)	F4−Ti1−F6	93.55(9)	F4−Ti1−F6	91.1
F3−Ti1−F7	94.05(13)	F5−Ti1−F6	93.67(10)	F5−Ti1−F6	91.1
F1−Ti2−F1B	82.93(17)	F1−Ti2−F2A	82.51(9)	F1−Ti2−F11	86.9
F1−Ti2−F4	86.23(14)	F1−Ti2−F7	86.15(10)	F1−Ti2−F7	88.9
F1−Ti2−F6	90.60(14)	F1−Ti2−F8	90.58(10)	F1−Ti2−F8	90.6
F1−Ti2−F6B	173.46(16)	F1−Ti2−F9	172.74(10)	F1−Ti2−F9	177.5
F1−Ti2−F4B	87.78(14)	F1−Ti2−F10	88.11(10)	F1−Ti2−F10	88.9
F1B−Ti2−F4	87.78(14)	F2A−Ti2−F7	86.74(10)	F11−Ti2−F7	88.9
F1B−Ti2−F6	173.46(16)	F2A−Ti2−F8	173.08(10)	F11−Ti2−F8	88.9
F1B−Ti2−F6B	90.60(14)	F2A−Ti2−F9	90.41(10)	F11−Ti2−F9	90.6
F1B−Ti2−F4B	87.78(14)	F2A−Ti2−F10	86.17(10)	F11−Ti2−F10	88.9
F4−Ti2−F6	92.74(16)	F7−Ti2−F8	92.43(11)	F7−Ti2−F8	91.1
F4−Ti2−F6B	92.62(15)	F7−Ti2−F9	91.85(10)	F7−Ti2−F9	91.1
F4−Ti2−F4B	172.00(20)	F7−Ti2−F10	171.41(10)	F7−Ti2−F16	176.9
F6−Ti2−F6B	95.88(24)	F8−Ti2−F9	96.48(11)	F8−Ti2−F9	91.9
F6−Ti2−F4B	92.62(15)	F8−Ti2−F10	94.02(11)	F8−Ti2−F10	91.1
F6B−Ti2−F4B	92.74(16)	F9−Ti1−F10	93.06(11)	F9−Ti2−F10	91.1
Ti1−F1−Ti2	164.40(19)	Ti1−F1−Ti2	154.16(13)	Ti1−F1−Ti2	176.9
Ti1−F1A−Ti2A	164.40(19)	Ti1−F2−Ti2A	160.53(12)	Ti1−F2−Ti1A	176.9

[a]Experimental geometrical parameters correspond to α- and β-$[ImH]_4[Ti_4F_{20}]$. [b]The atom-labeling schemes correspond to those used in Figure 10. [c]The SDDALL basis set was used.

hydrogen bonds (Table S4 in the Supporting Information). Each of the six cations is coordinated to two anions.

(e) $[ImH][Ti_2F_9]$. The smallest proportion of $[ImH]^+$ cations (Im:TiF_4 = 1:2) is observed in $[ImH][Ti_2F_9]$, which crystallized in two modifications (Figures 7 and 8). A high-temperature β-phase (structure determined at 298 K) crystallized in an orthorhombic unit cell, and a low-temperature α-phase (structure determined at 200 K) crystallized in a monoclinic unit cell. The crystallographically unique $[ImH]^+$ cation of the β-phase is 2-fold-disordered.

There is only one crystallographically independent titanium atom in the β-phase. The $[Ti_2F_9]^-$ anion is an infinite dimeric zigzag chain comprised of TiF_6 octahedra sharing vertices (Figure 7). Each TiF_6 octahedron shares three of its vertices with three other TiF_6 units so that each titanium atom is coordinated to three bridging [Ti−F_b, two within a chain, 1.9669(8) and 1.973(2) Å, and one between two polymeric chains, 1.979(2) Å] and three terminal [Ti−F_t, 1.763(2)−1.772(3) Å] fluorine atoms. Nearest-neighbor pairs of TiF_6 octahedra, belonging to different chains, coordinate to a single

dx.doi.org/10.1021/ic302468j | Inorg. Chem. 2013, 52, 8315−8326

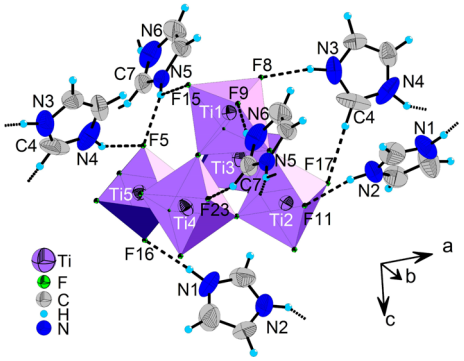

Figure 6. Crystal structure of $[ImH]_3[Ti_5F_{23}]$ showing coordination between the hydrogen atoms of the $[ImH]^+$ cations and the fluorine atoms of the $[Ti_5F_{23}]^{3-}$ anion. Thermal ellipsoids are drawn at the 50% probability level.

bridging $[ImH]^+$ cation through two crystallographically equivalent N−H···F (or C−H···F) hydrogen bonds [N1A···F2, 2.907(7) Å (or C2···F2, 2.992(7) Å); Table S4 in the Supporting Information].

The α-phase (Figure 8) is comprised of infinite dimeric chains consisting of crystallographically independent TiF_6 octahedra that coordinate to nearest-neighbor TiF_6 units in a manner similar to that observed in the β-phase. The Ti−F_t [1.768(2)−1.787(2) Å] and Ti−F_b [1.963(1)−1.991(1) Å] bond lengths are similar to the corresponding Ti−F bond lengths in $Cs[Ti_2F_9]$ at 200 K [Ti−F_t, 1.758(7)−1.790(7) Å; Ti−F_b, 1.955(3)−1.988(7) Å] and $[H_3O][Ti_2F_9]$ at 100 K [Ti−F_t, 1.754(2)−1.803(3) Å; Ti−F_b, 1.966(3)−2.004(2) Å].[4] Nearest-neighbor pairs of TiF_6 octahedra, belonging to different chains, coordinate to two different $[ImH]^+$ cations through two crystallographically inequivalent N1−H···F6 [N···F, 2.810(3) Å] and N2−H···F8 [N···F, 2.929(3) Å] hydrogen bonds (Table S4 in the Supporting Information); no $[ImH]^+$ bridging occurs between the octahedra of neighboring chains.

The Ti−F_b−Ti angles within the individual zigzag chains of the dimers are crystallographically equivalent in β-$[ImH][Ti_2F_9]$ [152.1(1)°], whereas these angles are comparable in α-$[ImH][Ti_2F_9]$ [149.54(8)° and 151.21(9)°]. The corresponding angles in $[H_3O][Ti_2F_9]$ and $Cs[Ti_2F_9]$ are more open [$[H_3O]^+$, 166.4(2)°; Cs^+, 156.3(4)°].[4] The Ti−F_b−Ti angles in $[ImH][Ti_2F_9]$, where the titanium atoms belong to two neighboring chains, are the same, within $\pm 3\sigma$ for the α-phase [162.27(8)°] and β-phase [163.1(2)°]. These angles are 143.7(2)° and 149.3(6)°, respectively, in the H_3O^+ and Cs^+ salts.[4]

In the case of $Cs[Ti_2F_9]$, the TiF_6 octahedra within one chain of the dimer are slightly rotated relative to those in the other chain (Figure 9a), with a dihedral angle of 22°. The corresponding dihedral angle (17°) of α-$[ImH][Ti_2F_9]$ (Figure 9c) results in $([Ti_2F_9]^-)_\infty$ chains of lower symmetry. In contrast, the TiF_6 octahedra of one chain eclipse those of the second chain in β-$[ImH][Ti_2F_9]$ (Figure 9d) and in $[H_3O][Ti_2F_9]$ (Figure 9b).

Computational Results. The gas-phase geometries of $[Ti_4F_{20}]^{4-}$ and $[Ti_5F_{23}]^{3-}$ were energy-minimized starting from the crystallographic coordinates and resulted in stationary points with all frequencies real. The B3LYP/SDDALL results are reported in Tables 3 and 4 and Figure 10. The energy-minimized geometry and vibrational frequencies (Table S5 in the Supporting Information) of $[TiF_6]^{2-}$ were also calculated (Ti−F, 1.893 Å) and served as a benchmark; the calculated Ti−F bond lengths are shown to be overestimated by 0.03 Å, whereas the Ti−F stretching frequencies are underestimated by ca. 40 cm^{-1}.

The calculated geometries of $[Ti_4F_{20}]^{4-}$ and $[Ti_5F_{23}]^{3-}$ are in good agreement with the experimental geometries, although all bond lengths are slightly overestimated, as observed for the $[TiF_6]^{2-}$ anion.

(a) $[Ti_4F_{20}]^{4-}$. All calculated terminal Ti−F bonds trans to terminal (Ti−F_{tt}) and bridging (Ti−F_{tb}) bonds are similar (1.839 and 1.842 Å, respectively), as observed experimentally [β, 1.803(3)−1.824(4) and 1.776(3)−1.793(3) Å; α, 1.800(2)−1.840(2) and 1.790(2)−1.817(2) Å, respectively; Table 3]. The Ti−F_b bonds are significantly longer (2.007 Å), in accordance with the experimental structure [β, 1.956(2)−1.978(2) Å; α, 1.965(2)−1.989(2) Å].

(b) $[Ti_5F_{23}]^{3-}$. The major features of the experimental $[Ti_5F_{23}]^{3-}$ anion structure are well reproduced, i.e., five TiF_6 units form a four-membered ring, with three of the TiF_6 units connected to a fifth TiF_6 unit through three F_b atoms. The terminal Ti−F_{tt} bond lengths that are trans to another terminal Ti−F_{tt} bond are longer than the terminal Ti−F_{tb} bond lengths that are trans to Ti−F_b bridge bonds, in accordance with the experimental bond lengths (Table 4). The bridging Ti−F_b bonds range from 1.930 to 2.054 Å [exptl, 1.946(2)−2.014(2) Å]. The Ti−F_{tt} and Ti−F_{tb} bonds are shorter than the analogous bonds in $[Ti_4F_{20}]^{4-}$. Experimentally, this trend is only apparent for the Ti−F_{tb} bonds. Among the F_b−Ti−F_b angles of the four-membered ring, the F2−Ti5−F18 angle (81.6°) is the smallest and is unique because F2 and F18 are not F-bridged to the triply F-bridged TiF_6 unit. The other F_b−Ti−F_b angles within the four-membered ring (av. 85.9°) are comparable to the F_b−Ti−F_b angles of the $[Ti_4F_{20}]^{4-}$ anion (av. 86.9°). The F_{tt}−Ti−F_{tt} angle is smaller (168.3°) in $[Ti_5F_{23}]^{3-}$ than that in $[Ti_4F_{20}]^{4-}$ (176.9°). The calculated angles are in good agreement with the experiment.

Raman Spectroscopy of β-$[ImH][Ti_2F_9]$, β-$[ImH]_4[Ti_4F_{20}]$, and $[ImH]_3[Ti_5F_{23}]$. The Raman spectra of β-$[ImH][Ti_2F_9]$ (Figure 11), β-$[ImH]_4[Ti_4F_{20}]$, and $[ImH]_3[Ti_5F_{23}]$ (Figures 12 and S9 and S10 in the Supporting Information) were acquired on randomly oriented single crystals. It was not possible to acquire usable spectra for the $[Ti_2F_{11}]^{3-}$ and $[TiF_6]^{2-}$ salts. As previously reported,[25] the frequency of the most intense Raman band can be used to identify complex titanium fluoride anions. This band corresponds to the symmetric in-phase terminal Ti−F stretching mode and has been shown to increase in frequency with increasing TiF_4 content and decreasing anion charge. The experimental Raman frequencies and intensities for the $[ImH]^+$ cation (Table S6 in the Supporting Information) compare well with previously published values[26] and are not discussed.

(a) $[Ti_2F_9]^-$. In contrast to the well-known $[TiF_6]^{2-}$ anion, and as previously observed for $[H_3O][Ti_2F_9]$[4] and $Cs[Ti_2F_9]$,[4] the Raman spectra of polymeric $[Ti_2F_9]^-$ anions are more complex (Figure 11) because the $([Ti_2F_9]^-)_n$ anions consist of infinite double chains of TiF_6 octahedra that share *cis*-vertices within each chain and because the component chains are joined by means of neighboring octahedra sharing a common vertex (Figure 7). The Raman spectrum of $Cs[Ti_2F_9]$ is the most complex, presumably because of the twisted orientation of the TiF_6 octahedra in one chain relative to those of the other chain. The twist results in symmetry lowering (i.e., the center of

dx.doi.org/10.1021/ic302468j | *Inorg. Chem.* 2013, 52, 8315−8326

Table 4. Experimental and Calculated Geometrical Parameters for the $[Ti_5F_{23}]^{3-}$ Anion

	exptl[a,b]	calcd (C_1)[b,c]		exptl[c]	calcd (C_1)[c]
		Bond Lengths (Å)			
Ti1−F4	1.985(2)	1.974	Ti3−F3	1.983(2)	2.010
Ti1−F15	1.770(2)	1.793	Ti3−F19	1.770(2)	1.803
Ti1−F14	1.942(2)	1.975	Ti3−F10	1.771(2)	1.795
Ti1−F9	1.769(2)	1.799	Ti4−F18	1.956(2)	1.932
Ti1−F8	1.785(2)	1.799	Ti4−F20	1.757(3)	1.796
Ti1−F1	1.971(2)	1.997	Ti4−F13	1.758(3)	1.795
Ti2−F3	1.982(2)	1.974	Ti4−F23	1.776(3)	1.803
Ti2−F1	2.007(2)	1.995	Ti4−F7	1.999(2)	2.007
Ti2−F7	1.946(2)	1.977	Ti4−F14	1.991(2)	2.011
Ti2−F11	1.784(2)	1.799	Ti5−F12	1.783(2)	1.812
Ti2−F22	1.761(2)	1.792	Ti5−F16	1.814(3)	1.826
Ti2−F17	1.772(2)	1.799	Ti5−F6	1.782(2)	1.812
Ti3−F21	1.769(4)	1.795	Ti5−F18	1.995(2)	2.054
Ti3−F2	1.961(2)	1.930	Ti5−F5	1.848(3)	1.826
Ti3−F4	1.980(2)	2.010	Ti5−F2	2.014(2)	2.051
		Bond Angles (deg)			
F15−Ti1−F4	89.01(11)	90.7	F10−Ti3−F2	89.45(11)	91.2
F14−Ti1−F4	86.84(11)	85.5	F3−Ti3−F4	83.35(9)	81.4
F9−Ti1−F4	172.05(12)	172.4	F19−Ti3−F4	90.10(12)	88.5
F1−Ti1−F4	82.09(9)	83.2	F10−Ti3−F4	168.89(11)	171.8
F8−Ti1−F4	87.69(11)	90.1	F19−Ti3−F3	88.53(11)	88.3
F15−Ti1−F14	89.33(10)	91.0	F10−Ti3−F3	88.45(11)	90.7
F9−Ti1−F15	98.20(11)	95.5	F19−Ti3−F10	97.21(12)	93.6
F15−Ti1−F1	168.75(11)	171.6	F20−Ti4−F18	90.17(12)	91.9
F15−Ti1−F8	95.50(11)	95.7	F13−Ti4−F18	90.11(12)	91.2
F9−Ti1−F14	89.87(11)	90.0	F23−Ti4−F18	169.52(12)	172.8
F14−Ti1−F1	83.36(9)	82.9	F18−Ti4−F7	84.27(10)	86.3
F8−Ti1−F14	172.64(11)	172.1	F18−Ti4−F14	82.47(10)	85.8
F9−Ti1−F1	90.35(10)	90.2	F20−Ti4−F13	98.40(13)	97.0
F9−Ti1−F8	94.92(12)	93.7	F20−Ti4−F23	95.99(14)	93.5
F8−Ti1−F1	91.01(10)	90.0	F20−Ti4−F7	171.01(12)	172.0
F3−Ti2−F1	82.23(9)	83.2	F20−Ti4−F14	91.22(12)	90.7
F7−Ti2−F3	83.49(10)	85.6	F13−Ti4−F23	97.33(13)	93.7
F11−Ti2−F3	169.75(12)	172.3	F13−Ti4−F7	88.70(12)	90.6
F22−Ti2−F3	89.71(11)	90.8	F13−Ti4−F14	167.89(12)	171.8
F17−Ti2−F3	89.52(11)	90.1	F23−Ti4−F7	88.52(12)	93.7
F7−Ti2−F1	83.94(10)	82.9	F23−Ti4−F14	88.92(12)	88.5
F11−Ti2−F1	88.64(11)	90.0	F14−Ti4−F7	81.07(10)	81.6
F22−Ti2−F1	170.90(11)	171.7	F12−Ti5−F16	96.13(12)	93.9
F17−Ti2−F1	87.38(10)	90.1	F6−Ti5−F12	96.43(12)	96.1
F22−Ti2−F7	90.99(12)	90.0	F12−Ti5−F18	172.33(11)	172.7
F11−Ti2−F7	90.95(11)	90.8	F6−Ti5−F5	90.76(11)	93.9
F17−Ti2−F7	169.51(11)	172.2	F12−Ti5−F2	89.60(10)	91.2
F22−Ti2−F11	99.02(13)	95.6	F6−Ti5−F16	96.43(12)	93.9
F17−Ti2−F11	94.72(11)	93.5	F16−Ti5−F18	86.25(11)	85.6
F22−Ti2−F17	96.81(12)	95.7	F16−Ti5−F5	169.57(11)	168.3
F21−Ti3−F2	90.26(11)	91.2	F16−Ti5−F2	85.68(11)	85.6
F21−Ti3−F4	91.90(11)	90.7	F12−Ti5−F5	90.55(12)	91.2
F21−Ti3−F3	173.84(11)	171.8	F6−Ti5−F18	90.53(11)	93.9
F19−Ti3−F21	95.41(13)	93.8	F6−Ti5−F2	173.35(11)	172.7
F10−Ti3−F21	95.73(12)	97.1	F5−Ti5−F18	86.13(11)	85.6
F2−Ti3−F4	82.42(10)	85.9	F18−Ti5−F2	83.30(10)	81.5
F2−Ti3−F3	85.26(10)	86.0	F5−Ti5−F2	86.37(10)	85.5
F19−Ti3−F2	170.77(11)	172.6			

[a]Experimental geometrical parameters correspond to $[ImH]_3[Ti_5F_{23}]$. [b]The atom-labeling schemes correspond to those used in Figure 10. [c]The SDDALL basis set was used.

symmetry of Ti_2F_9 is removed), and as a consequence, a larger number of vibrational bands is observed (Table 5).

(b) $[Ti_4F_{20}]^{4-}$ and $[Ti_5F_{23}]^{3-}$. The observed and calculated frequencies and detailed mode descriptions for $[Ti_4F_{20}]^{4-}$ and

dx.doi.org/10.1021/ic302468j | Inorg. Chem. 2013, 52, 8315−8326

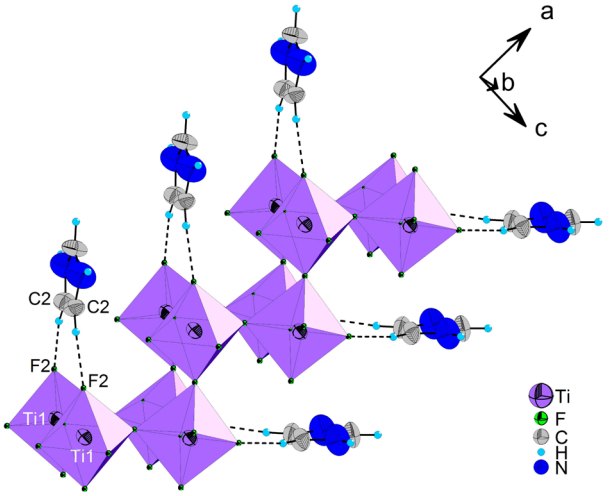

Figure 7. Crystal structure of β-[ImH][Ti_2F_9] showing coordination between the hydrogen atoms of the $[ImH]^+$ cations and the fluorine atoms of the $[Ti_2F_9]^-$ anion chains. Thermal ellipsoids are drawn at the 50% probability level. Only one of the two orientations of the disordered $[ImH]^+$ cations is depicted.

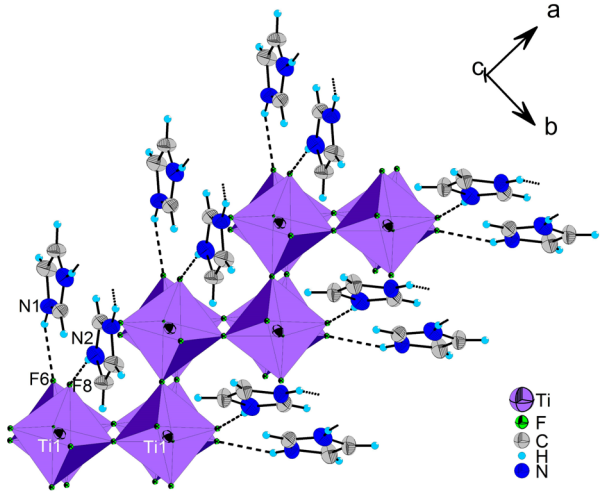

Figure 8. Crystal structure of α-[ImH][Ti_2F_9] showing coordination between the hydrogen atoms of the $[ImH]^+$ cations and the fluorine atoms of the $[Ti_2F_9]^-$ anion. Thermal ellipsoids are drawn at the 50% probability level. The Ti2 octahedra are eclipsed by the Ti1 octahedra and therefore are not labeled.

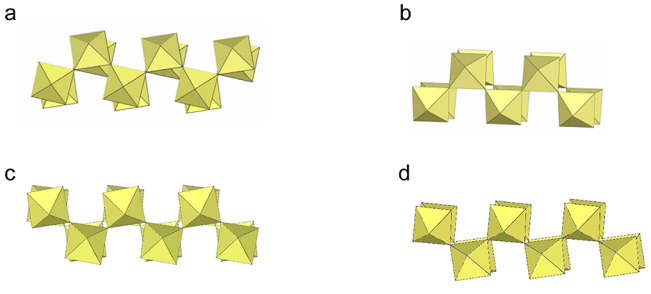

Figure 9. Infinite $([Ti_2F_9]^-)_\infty$ dimeric chains in the crystal structures of (a) Cs[Ti_2F_9], (b) [H_3O][Ti_2F_9], (c) α-[ImH][Ti_2F_9], and (d) β-[ImH][Ti_2F_9].

$[Ti_5F_{23}]^{3-}$ are provided in Tables 6 and 7 and S6 and S7 in the Supporting Information, respectively, where the atom numbering schemes correspond to those given in Figure 10. Spectral assignments for $[Ti_4F_{20}]^{4-}$ and $[Ti_5F_{23}]^{3-}$ were made by comparison with the calculated frequencies and Raman intensities of the energy-minimized gas-phase geometries, which are in good agreement with the experimental values at the B3LYP level of theory.

(i) $[Ti_4F_{20}]^{4-}$. The vibrational spectrum of $[Ti_4F_{20}]^{4-}$ was assigned under D_{2d} symmetry. A total of 66 fundamental vibrational modes belonging to the irreducible representations $10A_1 + 7B_1 + 16E + 7A_2 + 10B_2$ are expected, where the E and B_2 modes are both Raman- and IR-active, the A_1 and B_1 modes are Raman-active, and the A_2 modes are both Raman- and IR-inactive. The most intense band at 695 cm^{-1} is assigned to the totally symmetric Ti−F_{tb} stretch (F_{tb}, fluorine atom trans to a bridging fluorine atom), in good agreement with the calculated value (659 cm^{-1}), which is also predicted to be the most intense band in the Raman spectrum (Table 6). The bands at 560 and 624 cm^{-1} are assigned to the Ti−F_{tt} and Ti−F_{tb} (F_{tt}, fluorine atom trans to a terminal fluorine atom) symmetric and asymmetric stretching modes, respectively, and also compare well with the calculated values (547 and 604 cm^{-1}). The Ti−F_b stretches are predicted at ca. 450 cm^{-1} and are expected to be very weak in the Raman spectrum and are therefore unlikely to be observed. The remaining experimental bands at 189, 241, 271, 295, and 350 cm^{-1} are assigned to deformations that occur in the calculated frequency ranges.

(ii) $[Ti_5F_{23}]^{3-}$. The vibrational spectrum of $[Ti_5F_{23}]^{3-}$ was assigned under C_1 symmetry. A total of 78 fundamental Raman (IR) vibrational modes and bands are predicted. All bands that were calculated to be intense, were observed in the Raman spectrum. The most intense band at 741 cm^{-1} is assigned to the totally symmetric in-phase Ti−F_{tb} stretches, which is in very good agreement with the calculated frequency (732 cm^{-1}) and is also predicted to be the most intense band in the Raman spectrum (Table 7). The band at 717 cm^{-1} is assigned to the out-of-phase coupled Ti−F_{tb} and Ti−F_{tt} stretches, in good agreement with the predicted values at 700 and 710 cm^{-1}. The bands at 678 and 694 cm^{-1} are assigned to out-of-phase coupled Ti−F_{tt} stretches that are predicted to occur at 648, 678, and 681 cm^{-1}. The broad bands appearing at 476 and 562 cm^{-1} also involve Ti−F_b and Ti−F_{tb} out-of-phase and in-phase stretches, respectively. The medium-intensity band at 373 cm^{-1} is assigned to the δ(F_b−Ti−F_b) deformation, which is well reproduced by the calculation (366 cm^{-1}).

3. CONCLUSIONS

Although $[TiF_6]^{2-}$ salts are well-known, structural reports of poly[perfluorotitanate(IV)] anions were limited to $([TiF_5]^-)_\infty$,[11] $([Ti_2F_9]^-)_\infty$,[4] $[Ti_2F_{10}]^{2-}$,[7,8] $[Ti_2F_{11}]^{3-}$,[9] $([Ti_3F_{13}]^-)_\infty$,[12] $[Ti_4F_{18}]^{2-}$,[4,10] $[Ti_4F_{19}]^{3-}$,[19] $([Ti_7F_{30}]^{2-})_\infty$,[13] and $([Ti_8F_{33}]^-)_\infty$.[14] Investigations of the Im−TiF_4 system in aHF solvent have afforded five new salts, $[ImH]_2[TiF_6]\cdot 2HF$, $[ImH]_3[Ti_2F_{11}]$, $[ImH]_4[Ti_4F_{20}]$, $[ImH]_3[Ti_5F_{23}]$, and [ImH]-$[Ti_2F_9]$, where two of them have provided examples of new poly[perfluorotitanate] anions, namely, $[Ti_4F_{20}]^{4-}$ and $[Ti_5F_{23}]^{3-}$.

Quantum-chemical calculations using the B3LYP method have been used to obtain energy-minimized gas-phase geometries for the $[TiF_6]^{2-}$, $[Ti_4F_{20}]^{4-}$, and $[Ti_5F_{23}]^{3-}$ anions. The Raman spectra of the $[Ti_4F_{20}]^{4-}$ and $[Ti_5F_{23}]^{3-}$ anions have been assigned based on the calculated vibrational frequencies and vibrational displacements of their respective modes.

dx.doi.org/10.1021/ic302468j | Inorg. Chem. 2013, 52, 8315−8326

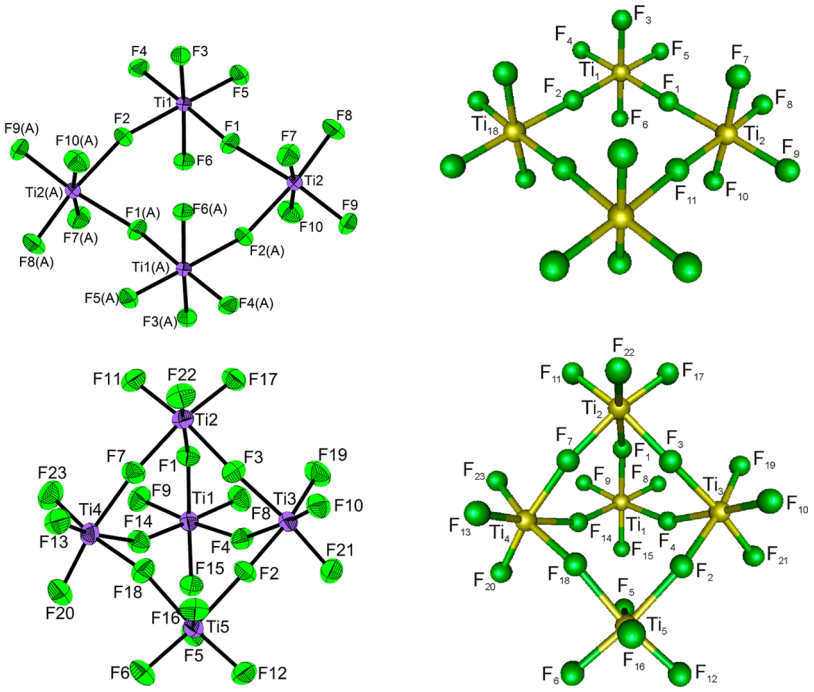

Figure 10. Experimental (left column) and calculated (right column; B3LYP/SDDALL) geometries of the $[Ti_4F_{20}]^{4-}$ and $[Ti_5F_{23}]^{3-}$ anions. The geometrical parameters are provided in Tables 3 and 4. Thermal ellipsoids are drawn at the 50% probability level.

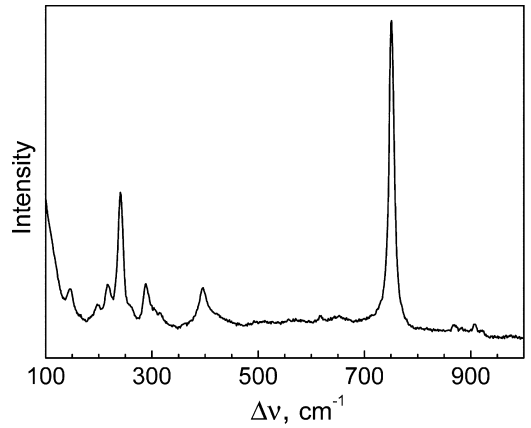

Figure 11. Raman spectrum of β-$[ImH][Ti_2F_9]$ recorded at room temperature on a randomly oriented single crystal sealed in a quartz capillary using 632.8-nm excitation.

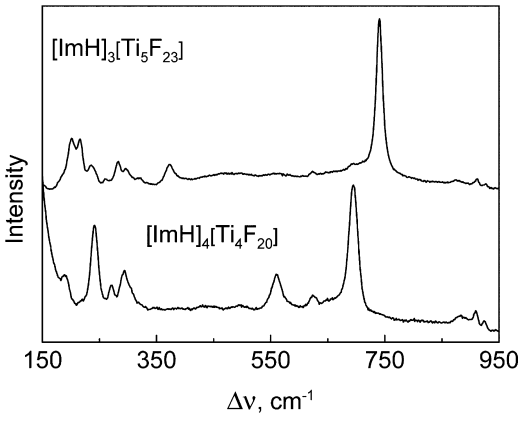

Figure 12. Raman spectra of $[ImH]_3[Ti_5F_{23}]$ and β-$[ImH]_4[Ti_4F_{20}]$ recorded at room temperature on randomly oriented single crystals sealed in quartz capillaries using 632.8-nm excitation.

4. EXPERIMENTAL SECTION

Reagents. Fluorine (Solvay Fluor and Derivate GmbH, Hannover, Germany), aHF (Linde AG, Puliach, Germany), and imidazole (Aldrich, 99%) were used. Titanium tetrafluoride was synthesized by the reaction of $TiCl_3$ (Sigma-Aldrich, 99.999%) with elemental fluorine F_2 in aHF. The purity of TiF_4 was confirmed by Raman spectroscopy and chemical analysis.

Synthetic Apparatus. All manipulations were carried out under anhydrous conditions. Volatile compounds, such as aHF and F_2, were handled on a vacuum line constructed from nickel/Teflon, and nonvolatile materials were handled in a drybox (M. Braun) in an argon atmosphere (<0.5 pmm H_2O). Single crystals of imidazolium poly[perfluorotitanates(IV)] were grown in T-shaped crystallization vessels comprised of two tetrafluoroethylene−hexafluoropropylene block copolymer (FEP; Polytetra GmbH, Germany) tubes (one 16-mm i.d. × 19-mm. o.d. and the other 4-mm i.d. × 6-mm. o.d.); each tube was heat-sealed on one end and joined at 90° through a Teflon T-connector. A Teflon valve was connected at 180° to the 19-mm-o.d. tube. Before use, the above-mentioned reaction/crystallization vessel assemblies were dried under dynamic vacuum and passivated with elemental fluorine at 1.1 bar for 2 h. Anhydrous HF (Linde, 99.995%) was treated with K_2NiF_6 (Advance Research Chemicals, Inc.) for several hours prior to use.

Crystal Growth of Imidazolium Poly[perfluorotitanates(IV)]. Stoichiometric amounts of imidazole and TiF_4 (totaling ca. 200 mg) were loaded into the 19-mm o.d. arm of the crystallization vessel inside a drybox (Table 8). The reagent mixture was then transferred to a metal/Teflon manifold, where aHF (5−7 mL) was condensed onto the starting material at −196 °C. The crystallization mixture was warmed to ambient temperature, and the resulting clear, colorless solution was decanted into the 6-mm o.d. side arm. Evaporation of the solvent from this solution was carried out by maintaining a temperature gradient of ca. 10−20 °C between the 6-mm o.d. (22−32 °C) and 19-mm o.d. (ca. 12 °C) tubes for several weeks. When the HF level in the smaller-diameter vessel ceased to further decrease, it was necessary to increase the temperature gradient. This was accomplished by slowly cooling the larger vessel in a cryostat from

dx.doi.org/10.1021/ic302468j | Inorg. Chem. 2013, 52, 8315−8326

Table 5. Experimental Raman Frequencies and Intensities for β-[ImH][Ti_2F_9] Compared with Those of Cs[Ti_2F_9] and [H_3O][Ti_2F_9][a]

β-[ImH][Ti_2F_9][b]	[H_3O][Ti_2F_9][c]	Cs[Ti_2F_9][c]
751(10)	756(10)	751(10)
		721(0.7)
		702(0.7)
		667(0.5)
		635(0.5)
396(1)	397(1)	397(1.5)
291(1)	293(1)	294(0.9)
		253(2)
241(3)	245(1.2)	241(1.9)
217(0.5)	229(1)	229(1.6)
		211(0.7)
198(0.1)	198 (sh)	
		170(0.5)
147(0.2)		

[a]Frequencies are given in cm^{-1}. [b]This work. [c]From ref 4.

+12 to −20 °C and then to −55 °C for [ImH]$_2$[TiF_6]·2HF. Several days to several weeks were required to induce crystallization. Slow distillation of aHF from the 6-mm o.d. tube into the 19-mm o.d. tube resulted in crystal growth inside the 6-mm o.d. tube. Selected single crystals were transferred to 0.3-mm quartz capillaries inside the drybox, and their Raman spectra were recorded at several random positions.

Raman Spectroscopy. Raman spectra with a resolution of 0.5 cm^{-1} were recorded at room temperature on a Horiba Jobin Yvon LabRam-HR spectrometer equipped with an Olympus BXFM-ILHS microscope. Samples were excited by the 632.8-nm emission line of a He−Ne laser with regulated power in the range 20−0.0020 mW, which gives 17−0.0017 mW focused on a 1 μm spot through a 50× microscope objective on the top surface of the sample.

Single crystals were mounted in the drybox in previously vacuum-dried quartz capillaries, which were initially sealed with Halocarbon 25-5S grease (Halocarbon Corp.) inside the drybox and later heat-sealed in an oxygen−hydrogen flame outside the drybox. Raman spectra of [ImH][Ti_2F_9], [ImH]$_3$[Ti_5F_{23}], and [ImH]$_4$[Ti_4F_{20}] were recorded at 17 mW with a 5 s exposure time for each scan. For [ImH]$_3$[Ti_5F_{23}] and [ImH]$_4$[Ti_4F_{20}], five scans, and for [ImH][Ti_2F_9], three scans were accumulated.

X-ray Crystal Structure Determinations. Crystals were immersed in perfluorodecalin (ABCR, 98%) inside a drybox, selected under a microscope, and mounted on the goniometer head of the diffractometer in a cold nitrogen stream. Although up to 15 crystals of consistent crystal habit were screened for each phase (Table 8), the

Table 7. Experimental and Calculated Vibrational Frequencies[a] and Intensities[b] for the [Ti_5F_{23}]$^{3-}$ Anion in [ImH]$_3$[Ti_5F_{23}]

exptl[c]	calcd[d]	assgnts (C_1)[e]
741(100)	732(85)[9]	ν(Ti-F_{tb})$_{ip}$
717[f]	710(4)[860]	ν(Ti-F_{tt})$_{oop}$ / ν(Ti-F_{tb})$_{oop}$
	710(5)[532]	
	700(3)[97]	ν(Ti-F_{tb})$_{oop}$
694(20)	681(5)[63]	ν(Ti-F_{tb})$_{oop}$
	681(5)[383]	
	678(2)[3]	ν(Ti-F_{tb})$_{oop}$ / ν(Ti-F_b)$_{ip}$
623(2)	658(2)[1052]	ν(Ti-F_{tb})$_{oop}$
	648(2)[554]	
562(1) br	592(4)[121]	ν(Ti-F_{tt})$_{ip}$ / ν(Ti-F_{tb})$_{ip}$ / ν(Ti-F_b)$_{ip}$
	562(4)[165]	ν(Ti-F_b)$_{ip}$ / ν(Ti-F_{tt})$_{ip}$
472[f]	501(12)[479]	ν(Ti-F_{tt})$_{ip}$ / ν(Ti-F_b)$_{oop}$
373(16)	366(8)[5]	δ(F_b-Ti-F_b) / δ(F_{tb}-Ti-F_{tb})
321(5)	324(<1)[<1]	δ(F_b-Ti-F_b)
297(10)	288(1)[118]	δ(F_b-Ti-F_b)
282(15)	282(2)[<1]	ρ_t(F_{tt}-Ti-F_{tt}) / ρ_r(F_{tb}-Ti-F_{tb})
	279(5)[23]	δ(F_b-Ti-F_b)
261(1)	256(<0.1)[12]	ρ_t(F_{tb}-Ti-F_b) / ρ_t(F_{tb}-Ti-F_{tb})
236(14)	225(1)[<0.1]	
	221(1)[<0.1]	
216(30)	212(2)[<1]	ρ_r(F_b-Ti-F_b)
202(30)	207(3)[<0.1]	ρ_t(F_{tb}-Ti-F_{tb})
	199(3)[<1]	

[a]Frequencies are given in cm^{-1}. The full set of calculated frequencies is reported in Table S8 (Supporting Information). [b]Values in parentheses denote relative Raman intensities. The abbreviation sh denotes a shoulder. Modes associated with the cation were also observed at 928(2), 912(5), and 876(2) cm^{-1}. [c]The Raman spectrum was recorded at ambient temperature on a randomly oriented single crystal sealed in a quartz capillary using 632.81-nm excitation. [d]The B3LYP/SDDALL method was used. Values in parentheses denote Raman intensities ($Å^4$ u^{-1}). Values in square brackets denote IR intensities (km mol^{-1}). [e]Vibrational assignments were based on modes calculated at the B3LYP level of theory. The abbreviations denote in-phase (ip), out-of-phase (oop), stretch (ν), bend (δ), rock (ρ_{rock}), torsion (ρ_t), a fluorine atom that is trans to a terminal fluorine atom (F_{tt}), a fluorine atom that is trans to a bridging fluorine atom (F_{tb}), and a bridging fluorine atom (F_b). [f]This band was visible for some crystals at specific orientations (Figure S10, Supporting Information).

Table 6. Experimental and Calculated Vibrational Frequencies[a] and Intensities[b] for the [Ti_4F_{20}]$^{4-}$ Anion in β-[ImH]$_4$[Ti_4F_{20}]

exptl[c]	calcd[d]		assgmnt (D_{2d})[e]
695(100)	659(70)[0]	A_1	ν_s(Ti−F_{tb})
624(12)	604(7)[0]	B_1	ν_{as}(Ti−F_{tb})
560(30)	547(22)[0]	A_1	ν_s(Ti−F_{tt})
350sh[f]	341(6)[0]	A_1	δ(F_{tt}−Ti−F_{tt})/δ(F_{tb}−Ti−F_{tb})/δ(F_b−Ti−F_b)
295(30)	299(2)[<0.1]	E	δ(Ti$F_{2tb}F_{2b}$)$_{umb}$
271(15)	277(4)[<0.1]	B_2	δ(F_{tt}−Ti−F_{tt})/δ(F_{tb}−Ti−F_{tb})
241(65)	233(5)[<1]	E	δ(F_{tt}−Ti−F_{tb})/δ(F_{tt}−Ti−F_b)/ρ_t(F_{tb}−Ti−F_b)
189(25)	170(3)[<0.1]	B_2	ρ_w(F_{tt}−Ti−F_{tt})/δ(F_{tb}−Ti−F_{tb})

[a]Frequencies are given in cm^{-1}. The full set of calculated frequencies is reported in Table S7 (Supporting Information). [b]Values in parentheses denote Raman intensities ($Å^4$ u^{-1}). Values in square brackets denote IR intensities (km mol^{-1}). [c]The Raman spectrum was recorded at ambient temperature on a randomly oriented single crystal sealed in a quartz capillary using 632.81-nm excitation. Values in parentheses denote relative Raman intensities. The abbreviation sh denotes a shoulder. Bands associated with the cation were also observed at 926(5), 908(10), and 882(5) cm^{-1}. [d]The B3LYP/SDDALL method was used. [e]Vibrational assignments were based on modes calculated at the B3LYP level of theory. The abbreviations denote symmetric (s), asymmetric (as), stretch (ν), bend (δ), wag (ρ_w), a fluorine atom that is trans to a terminal fluorine atom (F_{tt}), a fluorine atom that is trans to a bridging fluorine atom (F_{tb}), and a bridging fluorine atom (F_b). [f]This band was visible for some crystals at specific orientations (Figure S9 in the Supporting Information).

dx.doi.org/10.1021/ic302468j | Inorg. Chem. 2013, 52, 8315−8326

Table 8. Stoichiometries Used To Crystallize Imidazolium Poly[perfluorotitanates(IV)] and Phases Observed after Crystallization of Imidazole (Im) and TiF_4 in aHF

starting n(Im):n(TiF_4) molar ratios	phases observed after crystallization
2:1	$[ImH]_2[TiF_6]\cdot 2HF$, $[ImH]_3[Ti_2F_{11}]$
1.5:1	*a*
1:1	$[ImH]_4[Ti_4F_{20}]$, $[ImH]_3[Ti_5F_{23}]$
1:1.5	$[ImH]_4[Ti_4F_{20}]$, $[ImH]_3[Ti_5F_{23}]$, $[ImH][Ti_2F_9]$
1:1.67	$[ImH]_3[Ti_5F_{23}]$, $[ImH][Ti_2F_9]$
1:2	$[ImH][Ti_2F_9]$

[a]The nature of this phase is unknown because the single crystals that were grown were too small for an X-ray structure determination. In addition, Raman spectra could not be obtained because of an intense fluorescence background.

presence of other crystal phase(s) cannot be definitively ruled out. Data were collected at 200 or 298 K on a Rigaku AFC7 diffractometer equipped with a Mercury CCD area detector using graphite-monochromated Mo Kα radiation (λ = 0.71069 Å).

Processing of the raw data sets of $[ImH]_2[TiF_6]\cdot 2HF$, α-$[ImH]_4[Ti_4F_{20}]$, and α-$[ImH][Ti_2F_9]$ were completed using the *TEXSAN* package.[27] Processing of the raw data sets of $[ImH]_3[Ti_2F_{11}]$, β-$[ImH]_4[Ti_4F_{20}]$, $[ImH]_3[Ti_5F_{23}]$, and β-$[ImH][Ti_2F_9]$ were completed by using *APEX2 GUI* software,[28] which applied Lorentz and polarization corrections to three-dimensionally integrated diffraction spots. This was done after converting the data format from the Rigaku AFC7 to the Bruker APEX2 format. The program *SADABS*[29] was used for the scaling of diffraction data, the application of decay corrections, and empirical absorption corrections on the basis of the intensity ratios of redundant reflections. Although the data for $[ImH]_2[TiF_6]\cdot 2HF$ are not of good quality (see the CIF files in the Supporting Information), the authors are convinced that the structure solution is correct and have therefore integrated this result into the manuscript to provide a more comprehensive account.

In the case of $[ImH]_2[TiF_6]\cdot 2HF$, α-$[ImH]_4[Ti_4F_{20}]$, and α-$[ImH][Ti_2F_9]$, the *TEXSAN*[27] program was used to confirm the unit cell dimensions and the crystal lattices. In the case of $[ImH]_3[Ti_2F_{11}]$, β-$[ImH]_4[Ti_4F_{20}]$, $[ImH]_3[Ti_5F_{23}]$, and β-$[ImH][Ti_2F_9]$, the *XPREP*[30] program was used to confirm the unit cell dimensions and crystal lattices. The solutions were obtained by direct methods using the *SIR-92* (as implemented in the program package *WinGX*)[31] or the *SHELXTL-plus*[30,32] programs, which located the positions of the titanium and fluorine atoms. All further solution refinements were performed using the *SHELXTL-plus* program.[30] The positions of the remaining carbon and nitrogen atoms were revealed in successive difference Fourier syntheses. In the case of $[ImH]_2[TiF_6]\cdot 2HF$, $[ImH]_3[Ti_2F_{11}]$, β-$[ImH]_4[Ti_4F_{20}]$, and β-$[ImH][Ti_2F_9]$, 2-fold disorders had to be taken into account when refining some or all of the $[ImH]^+$ cations. Hydrogen atoms were included on idealized positions and allowed to ride on the atoms they were bonded to. The final refinements were obtained by introducing anisotropic thermal parameters and the recommended weightings for all atoms except the hydrogen atoms. The maximum electron densities in the final difference Fourier maps were located near the heavy atoms. The choices of space group were confirmed by *PLATON* from the *WinGX* software package.[31] Figures were prepared using the program *DIAMOND 3.1*.[33]

CCDC 907014 ($[ImH]_2[TiF_6]\cdot 2HF$), 907015 ($[ImH]_3[Ti_2F_{11}]$), 907016 (β-$[ImH]_4[Ti_4F_{20}]$), 907017 (α-$[ImH]_4[Ti_4F_{20}]$), 907018 ($[ImH]_3[Ti_5F_{23}]$), 907019 (β-$[ImH][Ti_2F_9]$), and 907020 (α-$[ImH][Ti_2F_9]$) contain the supplementary crystallographic data for this paper. These data can be obtained free of charge from The Cambridge Crystallographic Data Centre at www.ccdc.cam.ac.uk/data_request/cif.

Computational Methods. The optimized geometries and frequencies of the $[Ti_4F_{20}]^{4-}$ and $[Ti_5F_{23}]^{3-}$ anions were calculated at the B3LYP[34] level of theory. The Stuttgart semirelativistic large-core and effective-core pseudopotential basis sets (SDDall) augmented for fluorine, oxygen, and titanium atoms with two d-type polarization functions by Huzinaga et al.[35] were used.

Quantum-chemical calculations were carried out using the program *Gaussian 03*.[34] The levels and basis sets were benchmarked by calculating $[TiF_6]^{2-}$ (Table S5 in the Supporting Information). The geometries were fully optimized using analytical gradient methods. The vibrational frequencies were calculated at the B3LYP level using the appropriate minimized structure, and the vibrational mode descriptions were arrived at with the aid of *GaussView*.[36]

■ ASSOCIATED CONTENT

Ⓢ Supporting Information

List of geometrical parameters for $[ImH]_2[TiF_6]\cdot 2HF$ (Table S1) and α- and β-$[ImH][Ti_2F_9]$ (Tables S2 and S3), unit cells of $[ImH]_2[TiF_6]\cdot 2HF$ (Figure S1), $[ImH]_3[Ti_2F_{11}]$ (Figure S2), β-$[ImH]_4[Ti_4F_{20}]$ (Figure S3), α-$[ImH]_4[Ti_4F_{20}]$ (Figure S4), $[ImH]_3[Ti_5F_{23}]$ (Figure S5), β-$[ImH][Ti_2F_9]$ (Figure S6), and α-$[ImH][Ti_2F_9]$ (Figure S7), hydrogen-bonding geometries in α- and β-$[ImH][Ti_2F_9]$, $[ImH]_3[Ti_2F_{11}]$, α- and β-$[ImH]_4[Ti_4F_{20}]$, and $[ImH]_3[Ti_5F_{23}]$ (Table S4), geometries of $[Ti_2F_{11}]^{3-}$ anions (Figure S8), vibrational data for $[TiF_6]^{2-}$ (Table S5), Raman spectra of β-$[ImH]_4[Ti_4F_{20}]$ and $[ImH]_3[Ti_5F_{23}]$ (Figures S9 and S10), experimental vibrational frequencies for imidazolium cations in β-$[ImH][Ti_2F_9]$, β-$[ImH]_4[Ti_4F_{20}]$, and $[ImH]_3[Ti_5F_{23}]$ (Table S6); complete list of experimental and calculated vibrational frequencies for the $[Ti_4F_{20}]^{4-}$ and $[Ti_5F_{23}]^{3-}$ anions (Tables S7 and S8), complete ref 34, and X-ray crystallographic files in CIF format for the structure determinations of $[ImH]_2[TiF_6]\cdot 2HF$, α- and β-$[ImH][Ti_2F_9]$, $[ImH]_3[Ti_2F_{11}]$, α- and β-$[ImH]_4[Ti_4F_{20}]$, and $[ImH]_3[Ti_5F_{23}]$. This material is available free of charge via the Internet at http://pubs.acs.org.

■ AUTHOR INFORMATION

Corresponding Author

*E-mail: schrobil@mcmaster.ca (G.J.S.), zoran.mazej@ijs.si (Z.M.).

Notes

The authors declare no competing financial interest.

■ ACKNOWLEDGMENTS

I.M.S., E.A.G., and Z.M. gratefully acknowledge the Slovenian Research Agency (ARRS), and G.J.S. acknowledges the Natural Sciences and Engineering Research Council of Canada for a Discovery Grant for financial support of the present work. Calculations were carried out using facilities provided by the Shared Hierarchical Academic Research Computing Network (SHARCNET: www.Sharcnet.ca). The authors acknowledge Dr. James Britten of the McMaster University X-ray Facility for helping to convert Rigaku-formatted data to Bruker-formatted data.

■ REFERENCES

(1) Mizuta, S.; Shibata, N.; Ogawa, S.; Fujimoto, H.; Nakamura, S.; Toru, T. *Chem. Commun.* **2006**, 2575−2577.

(2) Qian, X.; Huang, J.; Qian, Y. *J. Organomet. Chem.* **2004**, *689*, 1503−1510.

(3) Murphy, E. F.; Murugavel, R.; Roesky, H. W. *Chem. Rev.* **1997**, *97*, 3425−3468.

(4) Mazej, Z.; Goreshnik, E. *Inorg. Chem.* **2009**, *48*, 6918−6923.

(5) Afanasiev, M. L.; Vasiliev, A. D.; Lisin, V. V.; Nazarov, A. M.; Sukhovskii, A. A. *J. Struct. Chem.* **1997**, *38*, 556−561.

(6) Lhoste, J.; Adil, K.; Leblanc, M.; Maisonneuve, V. *Acta Crystallogr., Sect. E* **2008**, *64*, 1375.
(7) Akutsu, H.; Ozeki, K.; Ozaki, T.; Nozawa, K.; Kinoshita, M.; Kozawa, K.; Uchida, T. *Bull. Chem. Soc. Jpn.* **1996**, *69*, 1869−1873.
(8) Dadachov, M. S.; Tang, L. Q.; Zou, X. D. *Z. Kristallogr. New Cryst. Struct.* **2000**, *215*, 605−606.
(9) Tang, L. Q.; Dadachov, M. S.; Zou, X. D. *Z. Kristallogr. New Cryst. Struct.* **2001**, *216*, 387−388.
(10) Decken, A.; Jenkins, H. D. B.; Knapp, C.; Nikiforov, G. B.; Passmore, J.; Rautiainen, J. M. *Angew. Chem., Int. Ed.* **2005**, *44*, 7958−7961.
(11) Cohen, S.; Selig, H.; Gut, R. *J. Fluorine Chem.* **1982**, *20*, 349−356.
(12) Mazej, Z.; Goreshnik, E. 19th International Symposium on Fluorine Chemistry, Jackson Hole, WY, Aug 23−28, 2009; Abstract No. 147.
(13) Müller, B. G. *J. Fluorine Chem.* **1981**, *17*, 489−499.
(14) Bialowons, H.; Müller, B. G. *Z. Anorg. Allg. Chem.* **1995**, *621*, 1223−1226.
(15) Hofmann, B. *Z. Anorg. Allg. Chem.* **1979**, *458*, 151−162.
(16) Marignac, C. *Ann. De Mines* **1859**, *15*, 269.
(17) Babel, D.; Tressaud, A. Crystal Chemistry of Fluorides. In *Inorganic Solid Fluorides*; Hagenmuller, P., Ed.; Academic Press Inc.: London, 1985; pp 175−178.
(18) Decian, P. A.; Fischer, J.; Weiss, R. *Acta Crystallogr.* **1967**, *22*, 340−343.
(19) Mazej, Z.; Goreshnik, E. *Eur. J. Inorg. Chem.* **2009**, 4503−4506.
(20) Mazej, Z.; Goreshnik, E. *Eur. J. Inorg. Chem.* **2008**, 1795−1812.
(21) Wilson, W. W.; Vij, A.; Vij, V.; Bernhardt, E.; Christe, K. O. *Chem.—Eur. J.* **2003**, *9*, 2840−2844.
(22) Aldous, D. W.; Stephens, N. F.; Lightfoot, P. *Dalton Trans.* **2007**, 2271−2282.
(23) Ross, C. R.; Paulsen, B. L.; Nielson, R. M.; Abrahams, S. C. *Acta Crystallogr., Sect. B: Struct. Sci.* **1998**, *54*, 417−423.
(24) Adil, K.; Leblanc, M.; Maisonneuve, V.; Lightfoot, P. *Dalton Trans.* **2010**, *39*, 5983−5993.
(25) Christe, K. O.; Schack, C. J. *Inorg. Chem.* **1977**, *16*, 353−359.
(26) Piecha, A.; Jakubas, R.; Pietraszko, A.; Baran, J.; Medycki, W.; Kruk, D. *J. Solid State Chem.* **2009**, *182*, 2949−2960.
(27) *TEXSAN for Windows: Single Crystal Structure Analysis Software*, version 1.06; Molecular Structure Corp.: The Woodlands, TX, 1997−1999.
(28) *APEX2*, release 2.0-2; Bruker AXS Inc.: Madison, WI, 2010.
(29) Sheldrick, G. M. *SADABS (Siemens Area Detector Absorption Corrections)*, version 2.10; Siemens Analytical X-ray Instruments, Inc.: Madison, WI, 2004.
(30) Sheldrick, G. M. *SHELXTL*, release 6.14; Siemens Analytical X-ray Instruments, Inc.: Madison, WI, 2008.
(31) Farrugia, L. J. *J. Appl. Crystallogr.* **1999**, *32*, 837−838.
(32) Sheldrick, G. M. *Acta Crystallogr., Sect. A* **2008**, *64*, 112−122.
(33) *DIAMOND*, version 3.1; Crystal Impact GbR: Bonn, Germany, 2004−2005.
(34) Frisch, M. J.; et al. *Gaussian 03*, revision D.01; Gaussian, Inc.: Wallingford, CT, 2004.
(35) Huzinaga, S.; Andzelm, J.; Kolobukowski, M.; Radzio-Andzelm, E.; Sakai, Y.; Tatewaki, H. *Gaussian Basis Sets for Molecular Calculations*; Physical Science Data 16; Elsevier: Amsterdam, The Netherlands, 1984.
(36) *GaussView*, release 3.0; Gaussian Inc.: Pittsburgh, PA, 2003.